Spatiotemporal PM$_{2.5}$ variations and its response to the industrial structure from 2000 to 2018 in the Beijing-Tianjin-Hebei region

Wenhao Xue [a], Jing Zhang [a, **], Chao Zhong [b], Xinyao Li [b], Jing Wei [a, c, *]

[a] College of Global Change and Earth System Science, Beijing Normal University, Beijing, China
[b] Business School, Beijing Normal University, Beijing, China
[c] Department of Atmospheric and Oceanic Science, Earth System Science Interdisciplinary Center, University of Maryland, College Park, MD, USA

ARTICLE INFO

ABSTRACT

The economy has developed rapidly in China during recent decades, especially in the Beijing-Tianjin-Hebei (BTH) region. Environmental problems have thus become increasingly prominent, particularly the presence of fine particulate matter with aerodynamic diameters $\leq$2.5 μm (PM$_{2.5}$). High-quality and high-resolution PM$_{2.5}$ data is urgently needed. Therefore, based on the newly released Moderate Resolution Imaging Spectroradiometer (MODIS) Multi-Angle Implementation of Atmospheric Correction (MAIAC) aerosol optical depth products, a high-quality PM$_{2.5}$ data set with a high spatial resolution of 1 km is first reconstructed covering 2000 to 2018 in the BTH region using the linear mixed effect (LME) model. This model shows an excellent performance with a high cross-validation coefficient of determination (R^2) of 0.85, a small root mean square error of 21.49 μg/m^3, and a small mean absolute error of 15.26 μg/m^3 from 2013 to 2018. It also has strong predictive power in estimating historical PM$_{2.5}$ concentrations, with a monthly R^2 equal to 0.72. There was a significant decreasing trend (i.e., -1.53 μg/m^3, p < 0.01) in PM$_{2.5}$ concentrations during the last two decades, and the largest downward trend (i.e., -6.83 μg/m^3, p < 0.01) occurred from 2013 to 2018. In addition, the response of PM$_{2.5}$ to the industrial structure is also examined using the vector autoregression model. In general, both the secondary industry and tertiary industry show significant influences and can contribute approximately 3.8% and 9.8% to the PM$_{2.5}$ pollution in the BTH region, respectively. This suggests that further industrial structural adjustment, e.g., clean energy production, or low-carbon technology development, is required for the future prevention and control of air pollution and the sustainable development of the economy.

© 2020 Elsevier Ltd. All rights reserved.

1. Introduction

In recent years, fine particulate matter with aerodynamic diameters $\leq$ 2.5 μm (PM$_{2.5}$) has become a national crisis in most developing countries, especially in China. Epidemiological studies have indicated that PM$_{2.5}$ is one of the major causes of cancer, heart and respiratory diseases (Song et al., 2019). In addition, approximately 0.7–2.2 million people die in China annually from problems related to air pollution (Rohde and Muller, 2015). The United Nations General Assembly proposed sustainable development goals (SDGs) as important health indicators related to air pollution, of which the values were extremely low in China in 2015 (Gupta and Vegelin, 2016). The Beijing-Tianjin-Hebei (BTH) region, which is one of the most important Chinese city clusters, has experienced rapid economic development, which has been accompanied by increasing air pollution, with severe fine particulate pollution episodes occurring over the recent decades (Bei et al., 2017; Xue et al., 2020; Tian et al., 2019). However, there were no real-time PM$_{2.5}$ monitoring stations in China before 2013, and the lack of historical PM$_{2.5}$ measurement records have limited studies of the air pollution impact on environmental economics and epidemiology.

Satellite remote sensing has been widely used in deriving ground-level PM$_{2.5}$ concentrations from aerosol optical depth (AOD) products due to their highly positive correlations (Wei et al., 2019a; Xin et al., 2016). There are numerous aerosol products with different spatiotemporal resolutions generated from multi-source satellites, including the Moderate-resolution Imaging Spectroradiometer (MODIS, Lee et al., 2011), Multi-angle Imaging

SpectroRadiometer (MISR, You et al., 2015), Visible Infrared Imaging Radiometer (VIIRS, Yao et al., 2019), and Himawari-8 (Zang et al., 2018). Among them, MODIS AOD products have been popularly adopted due to the satellite's mature aerosol retrieval algorithms, e.g., Dark Target (DT) and Deep Blue (DB), and long-term observations. However, these products are provided at low spatial resolutions of greater than 3 km and perform differently between global and regional areas (Wei et al., 2018; Wei et al., 2019c).

Three main approaches, including the physical, statistical and artificial intelligence models, have been widely used in establishing the $PM_{2.5}$-AOD relationships. The physical model is used to estimate $PM_{2.5}$ concentrations by correcting the humidity and height of the AOD but yields a poor performance due to its difficulty in explaining their complex relationships (Zhang and Li, 2015). An increasing number of statistical regression models, e.g., the geographically weighted regression (GWR, Song et al., 2014) model, the geographically and temporally weighted regression (GTWR, He and Huang, 2018) model, the linear mixed effect (LME, Ma et al., 2016) model, and the two-stage model (Ma et al., 2015), have been adopted to improve $PM_{2.5}$ estimates by introducing more potential influencing factors. These methods are fast and easy to implement and are often used for small- and medium-sized areas. In recent years, artificial intelligence models, e.g., random forest (Wei et al., 2019a), extremely randomized trees (Wei et al., 2019b; Wei et al., 2020), and deep brief networks (Li et al., 2017), have been applied in $PM_{2.5}$ estimates and achieved high accuracy due to their strong data mining ability. However, they require a large number of training samples and are thus often used for large-scale areas.

There are also many studies exploring the potential impact of $PM_{2.5}$ pollution from both natural and human aspects (Yang et al., 2018; Zhang et al., 2018b; Wu et al., 2018). Meteorological factors and topography show large influences on $PM_{2.5}$ pollution from the local to national scales in China, exhibiting significant seasonal variations (Yang et al., 2017). However, $PM_{2.5}$ pollution appears to be closely related to socio-economic factors. Zhang et al. (2018b) pointed out that air quality policies are mainly determined by the economic development in most provinces in China. In addition, the economic/population scale, urbanization level, industrialization level, and energy utilization efficiency have been proven to be the main driving forces behind the increasing $PM_{2.5}$ concentrations (Luo et al., 2018). Moreover, the importance of socio-economic factors to $PM_{2.5}$ pollution has been investigated using the Stochastic Impacts by Regression on Population Affluence and Technology model, and secondary industry shows the greatest impact. Furthermore, changes in the industrial structure also determine the diversity of CO_2 emissions and water resource constraints in the BTH region, causing indirect effects on air pollution (Chen et al., 2019; Ding et al., 2019).

Over the years, although there has been an increasing number of studies on spatiotemporal $PM_{2.5}$ estimations and variations from the local to national scales in China, these studies have mainly focused on developing new methods to improve the accuracy of $PM_{2.5}$ estimates for years with sufficient $PM_{2.5}$ ground monitoring stations since 2013. Therefore, the generated $PM_{2.5}$ data sets cover short periods of one or a couple of years, and few studies have examined the long-term historical $PM_{2.5}$ variations in China (Ma et al., 2015; Xue et al., 2020). Additionally, the AOD products adopted for the $PM_{2.5}$ estimations have coarse spatial resolutions and show large uncertainties over bright surfaces, especially for urban areas (Wei et al., 2018, 2019d). Therefore, these data sets always yield poor-quality data at low spatial resolutions, limiting their applications in medium- and small-scale areas. Those also limit the study of the influence and response mechanisms of the economy, health and other factors affecting $PM_{2.5}$ pollution, especially for main urban agglomerations (e.g., the BTH region) in China.

Therefore, the purpose of this study is to reconstruct a long-time series and high-spatial-resolution $PM_{2.5}$ data set in the BTH region. For this purpose, the newly released MAIAC AOD products with a 1 km spatial resolution combined with meteorological and land cover data are employed, and the longest-period (2000−2018) and highest-resolution (1 km) $PM_{2.5}$ data set is first generated using the LME model. Then, the historical spatial distributions and temporal variations in $PM_{2.5}$ pollution are fully investigated under the Five-Year Plans (FYPs) implemented by the Chinese government. In addition, the dynamic relationships and interactions between the industrial structure and $PM_{2.5}$ pollution are also explored in the BTH region using the vector auto regression (VAR) model. Our study can provide measures and suggestions for the local government for future air pollution prevention and control. Section 2 describes the study and data sources and integration. Section 3 introduces the $PM_{2.5}$ estimation method, section 4 presents the validation of $PM_{2.5}$ estimates and the long-term spatiotemporal variations, and section 5 investigates the effects of industrial structure on $PM_{2.5}$ pollution in the BTH region. Section 6 provides some policy suggestions, and section 7 gives the summary and conclusions.

2. Materials

2.1. Study area

One of the main urban agglomerations in China, i.e., BTH ($113.45°−119.85°$ E, $36.04°−42.62°$ N), was selected, which includes Beijing, Tianjin and 11 cities in Hebei province. This region covers 218,000 km^2 with a total population of 110 million inhabitants. In 2011, the BTH region was designated as the Capital Economic Circle by the National Development and Reform Commission, and a high GDP level of 7461.26 billion yuan was attained, accounting for 10% of the total GDP of China. Fig. 1 shows the geographical location and
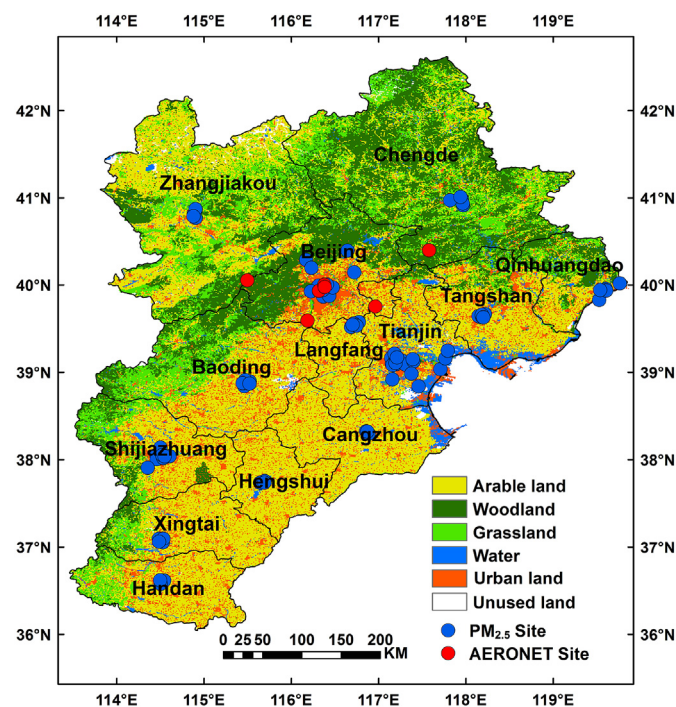

Fig. 1. Spatial distribution of the $PM_{2.5}$ monitoring and Aerosol Robotic Network (AERONET) sites in the Beijing-Tianjin-Hebei region. The background map represents the land use cover.

land use cover of the BTH region in China. Urban areas and croplands are the two main land use types in this area, occupying approximately 46% and 13%, respectively, of the total area. Remarkably, industrial and residential pollutant emissions are the main sources of $PM_{2.5}$ pollution in this region, with only 30% transferred from surrounding areas affected by meteorological conditions (Li et al., 2015). Moreover, a wide range of emissions sources produce a variety of $PM_{2.5}$ components, including toxic heavy metals (e.g., arsenic, cadmium, and chromium), secondary inorganic ions (SO_4^{2-}, NO^{3-}, and $NH4^+$), organic carbon (OC) and elemental carbon (EC). Thus, serious air pollution easily occurs, especially in winter (Gao et al., 2018).

2.2. Data sources

2.2.1. $PM_{2.5}$ ground measurements

Records of hourly $PM_{2.5}$ in situ measurements for 2013–2018 from 79 monitoring stations (Fig. 1) in the BTH region are collected. These monitoring stations are evenly distributed and cover almost all cities in the BTH region. Values that remained constant for three consecutive hours due to instrument failure were removed first, and the daily $PM_{2.5}$ values were averaged from all available hourly $PM_{2.5}$ observations during the daytime for each day in our study.

2.2.2. MODIS MAIAC AOD products

Both Terra and Aqua MODIS released new Collection 6 1 km MAIAC AOD products (Lyapustin et al., 2018) from 2000 to 2018 covering the BTH region, which were obtained to estimate the historical $PM_{2.5}$ records. First, Terra and Aqua daily MAIAC AOD retrievals at 550 nm are combined to increase the spatial coverage using established linear transformation models (Wei et al., 2020). Real-time AOD measurements from seven available Aerosol Robotic Network (AERONET) sites (Fig. 1) in the BTH region were chosen to validate the reliability of the MAIAC AOD retrievals using the spatiotemporal matching approach (Wei et al., 2018, 2019c). The results illustrated that the MAIAC AOD retrievals are highly consistent with the AERONET AODs (Fig. S1), with a notable slope of 0.96 and a high R^2 value of 0.89. The root mean square error (RMSE) and mean absolute error (MAE) are 0.21 and 0.11, respectively.

2.2.3. Auxiliary data

To further determine the relationship between AOD and $PM_{2.5}$, meteorological data was employed. In this study, eight meteorological variables, including the boundary layer height (BLH), evaporation (ET), total precipitation (PRE), relative humidity (RH), surface pressure (SP), 2 m temperature (TEM), wind direction (WD) and wind speed (WS), at a spatial resolution of 0.125 ° × 0.125 ° were collected from ERA-Interim atmospheric reanalysis products (Dee et al., 2011). Moreover, the MODIS monthly 1 km-resolution normalized difference vegetation index (NDVI) product was also used to reflect the vegetation conditions on the land surface. In addition, to ensure spatial and temporal resolution consistency among all variables, all auxiliary data were interpolated to a uniform scale of 1 km for each day using the bilinear interpolation method.

2.2.4. Socioeconomic data

The provincial quarterly growth values of the secondary industry (SI) and tertiary industry (TI) in the BTH region from 2000 to 2017 were collected. The SI and TI output data were collected from the National Bureau of Statistics (NBS) database. Moreover, the ratio of $PM_{2.5}$ to GDP ($GPM_{2.5}$) was used to represent the changes in the $PM_{2.5}$ concentration caused by economic growth, with the same spatial and temporal resolution as those of the SI and TI. GDP data were obtained from the Statistical Yearbook pertaining to the BTH region.

3. Methodology

3.1. Model development

In this study, the LME model was selected to determine the relationships between the surface $PM_{2.5}$ measurements and all independent variables for each year from 2013 to 2018, separately. Then, the 2013 LME model was employed to predict the historical $PM_{2.5}$ concentrations from 2000 to 2012. The LME model includes fixed and random effects that suitably explained the spatiotemporal variations between the $PM_{2.5}$ concentration and the other independent variables, which can be expressed as follows:

$$
\begin{aligned}
PM_{2.5jt} &= (\beta_0 + \beta_{0t} + \beta_{0m} + \beta_{0s}) + (\beta_1 + \beta_{1t}) \times AOD_{jt} + (\beta_2 + \beta_{2t}) \\
&\times BLH_{jt} + (\beta_3 + \beta_{3t}) \times RH_{jt} + (\beta_4 + \beta_{4m}) \times NDVI_{jm} + (\beta_5 + \beta_{5s}) \\
&\times ET_{jt} + (\beta_6 + \beta_{6s}) \times PRE_{jt} + (\beta_7 + \beta_{7s}) \times SP_{jt} + (\beta_8 + \beta_{8s}) \\
&\times TEM_{jt} + (\beta_9 + \beta_{9s}) \times WD_{jt} + (\beta_{10} + \beta_{10s}) \times WS_{jt} \\
&+ \varepsilon_{1jt}(\beta_{0t}, \beta_{1t}, \beta_{2t}, \beta_{3t}) \\
&\sim N[(0,0,0,0), \psi_1] + \varepsilon_{2jm}(\beta_{0m}, \beta_{4m}) \\
&\sim N[(0), \psi_2] + \varepsilon_{3js}(\beta_{5s}, \beta_{6s}, \beta_{7s}, \beta_{8s}, \beta_{9s}, \beta_{10s}) \\
&\sim N[(0,0,0,0,0,0), \psi_3]
\end{aligned}
$$

$$[1]$$

where $PM_{2.5jt}$ is the ground-based measured $PM_{2.5}$ concentration in grid j on day t, β_0 is the fixed intercept, and β_{0t}, β_{0m}, and β_{0s} are the daily, monthly and seasonal random intercepts, respectively. AOD_{jt}, BLH_{jt}, RH_{jt}, ET_{jt}, PRE_{jt}, SP_{jt}, TEM_{jt}, WD_{jt} and WS_{jt} denote the appropriate variable factors in grid j on day t. In addition, $NDVI_{jm}$ is the NDVI in grid j for month m. β_1-β_{10} represent the fixed slopes of each independent variable, and β_{1t}-β_{3t}, β_{4m}, and β_{5s}-β_{10s} are the daily, monthly, and seasonal random slopes, respectively, while ε_{1jt}, ε_{2jm} and ε_{3js} are the error terms at the daily, monthly and seasonal scales in grid j. N indicates the normal distribution for all variables, and ψ_1, ψ_2 and ψ_3 are the variance-covariance matrices for all random effects at the daily, monthly and seasonal levels, respectively.

In this study, the commonly used sample-based 10-fold cross validation (CV) approach is selected to evaluate the goodness of fit and prediction performance of the LME model (Kohavi, 1995). In addition, several statistical indicators, e.g., the linear regression equation, coefficient of determination R^2, RMSE, and MAE, are calculated to represent the model accuracy and estimate the uncertainty.

3.2. Data analysis method

To explore the temporal trends of air pollution, the monthly $PM_{2.5}$ values were first deseasonalized by calculating the monthly anomalies and then used to calculate the linear trends. An anomalous $PM_{2.5}$ concentration was defined as the difference between the monthly mean value in one year and the monthly $PM_{2.5}$ average over the whole period. Then the ordinary least squares fitting method was selected to calculate the linear $PM_{2.5}$ trend (Wei et al., 2019e). Moreover, the paired-samples T-test was selected to evaluate the statistical significance of the trends. Noticeably, the spurious regression phenomenon has been widely encountered in traditional long time-series economic studies (Granger and Newbold, 1974), leading to contradictory or incorrect results. To avoid such issues, the unit root test should be selected to evaluate the stationarity and integration of all socioeconomic data.

There are three specific tests that have been widely applied to test the unit root, including the Augmented Dickey-Fuller (ADF) test, the Phillips-Perron (PP) test, and the Dickey-Fuller (DF) test. Among them, the ADF test has been proven to be more effective and robust, especially for data with a small sample size. However, the sum-of-covariance for long-term variation is required for both the PP and DF tests (Cavaliere and Xu, 2014). Thus, the ADF test was selected for the unit root test in this study.

In this study, the vector auto regression (VAR) model was adopted to predict and assess the strength and duration of the dynamic interactions among $GPM_{2.5}$, SI and TI. The VAR model is a multivariate model constructed with endogenous variables and lagged values of the endogenous variables. However, the ADF test mainly expresses the long-term equilibrium relationship among all variables, and sequential causality may exist. Therefore, before building this model, the Granger causality test was selected to determine the causal relationship with 1−4 lags (Granger, 1969; Sims, 1972).

In addition, the sequential modified linear regression test statistic (LR), final prediction error (FPE), Akaike information criterion (AIC), Schwarz criterion (SC) and Hannan-Quinn information criterion (HQIC) were selected to determine the lag order of the model (Lütkepohl, 1985; Hurvich and Tsai, 1993). In this study, the impulse response function was applied to explain the dynamic effects of the independent variables, which can be expressed as:

$$
\begin{aligned}
GPM_{2.5} = &\, a_{11}GPM_{2.5t-1} + a_{12}GPM_{2.5t-2} + a_{13}GPM_{2.5t-3} \\
&+ a_{14}GPM_{2.5t-4} + b_{11}SI_{t-1} + b_{12}SI_{t-2} + b_{13}SI_{t-3} + b_{14}SI_{t-4} \\
&+ c_{11}TI_{t-1} + c_{12}TI_{t-2} + c_{13}TI_{t-3} + c_{14}TI_{t-4} + u_1
\end{aligned}
$$
[2]

$$
\begin{aligned}
SI = &\, a_{21}GPM_{2.5t-1} + a_{22}GPM_{2.5t-2} + a_{23}GPM_{2.5t-3} \\
&+ a_{24}GPM_{2.5t-4} + b_{21}SI_{t-1} + b_{22}SI_{t-2} + b_{23}SI_{t-3} + b_{24}SI_{t-4} \\
&+ c_{21}TI_{t-1} + c_{22}TI_{t-2} + c_{23}TI_{t-3} + c_{24}TI_{t-4} + u_2
\end{aligned}
$$
[3]

$$
\begin{aligned}
TI = &\, a_{31}GPM_{2.5t-1} + a_{32}GPM_{2.5t-2} + a_{33}GPM_{2.5t-3} \\
&+ a_{34}GPM_{2.5t-4} + b_{31}SI_{t-1} + b_{32}SI_{t-2} + b_{33}SI_{t-3} + b_{34}SI_{t-4} \\
&+ c_{31}TI_{t-1} + c_{32}TI_{t-2} + c_{33}TI_{t-3} + c_{34}TI_{t-4} + u_3
\end{aligned}
$$
[4]

where a_{ij}, b_{ij}, and c_{ij} ($i = 1, 2, 3; j = 1, 2, 3, 4$) are pending parameters, $GPM_{2.5t-j}$, SI_{t-j} and TI_{t-j} ($t = 1, 2, \ldots, 72$) are endogenous variables at lag j, and u_i is the disturbance. The mathematical expectation of the disturbance terms is 0. Moreover, variance decomposition was performed to examine the $GPM_{2.5}$, SI and TI variations.

4. Results and discussion

4.1. Correlation and collinearity diagnosis

The MAIAC AOD products were first validated against AERONET AOD ground measurements (Wei et al., 2019c) at 18 monitoring stations (marked as red dots in Fig. 1) from 2015 to 2018 in China (Fig. S1). For this, there were a total of 4251 collected matchups between MAIAC and AERONET AODs using the spatiotemporal matching approaches (Wei et al., 2019c,d) across China. The results show that the MAIAC AODs agree well with AERONET AODs ($R = 0.961$) with an overall high accuracy (i.e., MAE = 0.068, RMSE = 0.121). About 84% of the matchups fall within the MODIS expected errors (EE, $\pm (0.05 + 15\%)$) at the national scale. Besides

vegetated surfaces, e.g., cropland and grassland, the MAIAC algorithm shows considerable accuracy, with about 85% of the matchups falling within the EE envelope over heterogeneous urban surfaces. Compared to our previous studies, the MAIAC AOD products are much better and less biased than the widely used Dark Target and Deep Blue AOD products, especially for urban areas (Wei et al., 2019a, e). Thus, the MAIAC products at a higher 1 km resolution, rather than DT and DB AOD products at coarser 3−10 km resolutions, were selected, which can lead to more accurate and detailed $PM_{2.5}$ estimations.

Before model building, the potential relationships among the $PM_{2.5}$ measurements and all independent variables were calculated (Table S1). Except for PRE, all the other variables were significantly correlated with the $PM_{2.5}$ measurements at the 99% confidence level ($p < 0.01$) for each year in China. Among all the variables, positive effects of the AOD, ET, RH, and SP on the $PM_{2.5}$ concentration existed, whereas the remaining variables had negative effects. In general, the AOD exhibited the highest correlation with the $PM_{2.5}$ concentration ($R = 0.48-0.57$), while the PRE had the lowest correlation ($R = -0.021$ to -0.07).

In addition, to avoid errors due to potential multicollinearity among the large number of independent variables, the variance inflation factor (VIF) was calculated in this study (Table S2). The results indicated that no multicollinearity issue existed among the selected variables with VIF values < 10 (Neter et al., 1996). The descriptive statistics for all variables are also provided (Table S3), and the annual mean $PM_{2.5}$ concentration was $67.65 \pm 60.67 \, \mu g/m^3$ from 2013 to 2018 in the BTH region, China, which is much higher than the limits defined in the National Ambient Air Quality Standard (i.e., $PM_{2.5} = 35 \, \mu g/m^3$).

4.2. Model fitting and validation

Fig. 2 shows the 10-fold cross-validation results in the BTH region for each year from 2013 to 2018. In addition, the model-fitted results are also depicted in Fig. S2. The results illustrated that the LME model exhibited an excellent performance in capturing the daily $PM_{2.5}$ concentration, with model-fitting R^2 values of $0.83-0.91$ and model-CV R^2 values of $0.80-0.89$, indicating that the $PM_{2.5}$ estimates were neither dramatically under- nor over-fitted. Among the different years, the LME model had the best performance in 2018, with the highest CV-R^2 value of 0.89 and the smallest RMSE and MAE values of 13.92 and $9.83 \, \mu g/m^3$, respectively, between the measured and estimated $PM_{2.5}$ in the BTH region. This was mainly due to the low-level $PM_{2.5}$ pollution, with approximately 89% of the data samples $< 100 \, \mu g/m^3$. In contrast, the worst performance was observed in 2014, with the lowest CV-R^2 value and largest estimation uncertainties (i.e., RMSE = 28.4 $\mu g/m^3$ and MAE = 20.41 $\mu g/m^3$). The primary reason is that the air pollution was more severe in this year, with more than 27% of the data samples $> 100 \, \mu g/m^3$, and relatively discrete data samples may have increased the difficulty of model fitting (Wei et al., 2019b). In general, the LME model is robust and can suitably estimate the daily $PM_{2.5}$ concentrations (e.g., $R^2 > 0.80$, RMSE $< 29 \, \mu g/m^3$, and MAE $< 21 \, \mu g/m^3$) in the BTH region.

Then, the LME-based $PM_{2.5}$-AOD relationships were used to estimate the historical $PM_{2.5}$ records for 2000−2012 in the BTH region. However, there were no $PM_{2.5}$ measurements before 2013; thus, to test the predictive power of the LME model, the daily $PM_{2.5}$ concentrations in 2013 were estimated using the LME model established in 2014, and the estimations of $PM_{2.5}$ were validated against the $PM_{2.5}$ observations in 2013. The results indicate that the LME model can correctly capture 41% of the historical daily $PM_{2.5}$ concentrations. More importantly, the monthly and seasonal $PM_{2.5}$ estimates were highly consistent with the surface measurements,
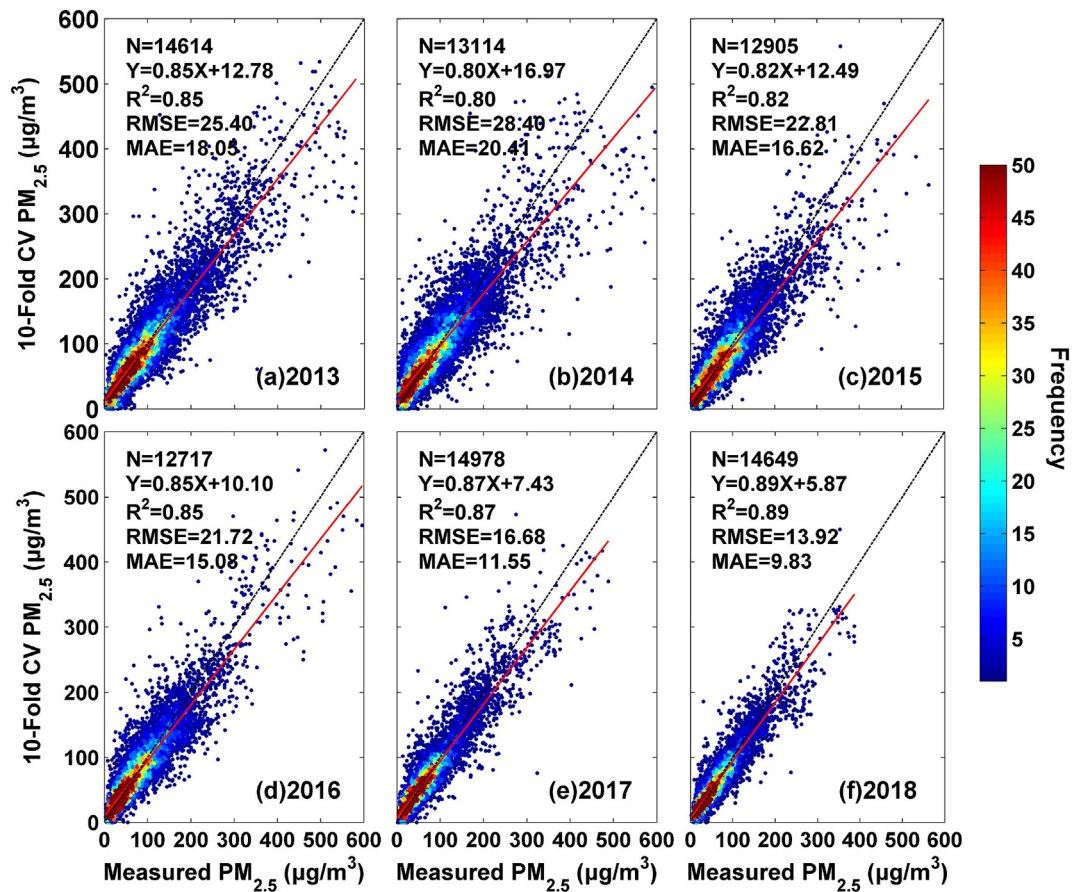
Fig. 2. Density scatterplots of the 10-fold cross-validation results for the LME model from 2013 to 2018 in the Beijing-Tianjin-Hebei region, China. The red and black lines indicate the regression fitting and 1:1 lines, respectively. (For interpretation of the references to colour in this figure legend, the reader is referred to the Web version of this article.)

with high R^2 values of 0.72 and 0.80, small RMSE values of 18.75 and 15.57 $\mu g/m^3$, and small MAE values of 17.96 and 14.90 $\mu g/m^3$, respectively. These findings suggest that the LME model has a good prediction ability and can be used to reconstruct the historical PM$_{2.5}$ records in the study area.

4.3. Spatial distribution from 2000 to 2018

Fig. 3 shows the spatial distribution of the seasonal average PM$_{2.5}$ concentrations in the BTH region from 2000 to 2018. The mean PM$_{2.5}$ concentrations were 52.76, 49.09, 58.41 and 82.72 $\mu g/m^3$ for spring, summer, autumn and winter, respectively. The highest PM$_{2.5}$ concentration occurred in winter and was 36.22%, 40.7% and 29.4% higher than those in the other three seasons. Crop residue burning and fossil fuel combustion are the main reasons for the increase in PM$_{2.5}$, especially during the heating period (Zhang et al., 2017). In all four seasons, the northern region of BTH is characterized by low PM$_{2.5}$ levels. The main reason for this result is that there are fewer human activities in this area, and the main land use types are forests and grasslands. In contrast, high PM$_{2.5}$ levels occurred in the southern BTH region, where most cities of Hebei province are located. A high urbanization level, massive industrial production and sparse vegetation coverage resulted in the high PM$_{2.5}$ concentrations. Therefore, over the whole study period, the spatial distribution of PM$_{2.5}$ is closely associated with human activities and land cover. Topography can also play a crucial role in affecting the spatial distribution in PM$_{2.5}$ concentrations associated with meteorology, wherein high-level PM$_{2.5}$ concentrations are

prone to occur over the southeast plain areas, while low PM$_{2.5}$ concentrations are mainly observed in northwest mountainous regions (Wang et al., 2018). However, significant PM$_{2.5}$ spatial distribution distinctions existed in BTH during different time intervals.

Four time periods were selected for PM$_{2.5}$ spatial variation analysis according to the Five-Year Plans (FYPs) in China. The FYP is an important part of the national economic plan of China. During the 11th FYP (2006–2010), primary industrial air pollutant emissions, e.g., SO$_2$, NO$_2$, smoke, and dust, were reduced in the BTH region due to the implemented structural management measures. To mitigate air pollution problems, a transformation of energy production and utilization was carried out during the 12th FYP (2011–2015) in China. Additionally, the government has continued to accelerate the development of strategic emerging industries in the 13th FYP (2016–2020) (Zhang et al., 2018a). Fig. 4 shows the spatial distributions of the annual average PM$_{2.5}$ concentrations from 2000 to 2005 (9th and 10th FYPs), 2006–2010 (11th FYP), 2011–2015 (12th FYP) and 2016–2018 (13th FYP). Similar to the seasonal spatial distributions, the southern BTH region was more polluted than the northern region, with higher PM$_{2.5}$ concentrations in all time periods. The highest PM$_{2.5}$ concentration was recorded in the 11th FYP period, with the mean concentration of 85.14 $\mu g/m^3$ across the BTH region. In this period, the BTH metropolitan area was established to develop the economy. This resulted in serious air pollution problems, and the annual PM$_{2.5}$ concentration in all BTH areas was higher than 35 $\mu g/m^3$. In contrast, the cleanest air conditions occurred in the 13th FYP, with the annual mean PM$_{2.5}$ concentration in 29.78% of the area being lower than
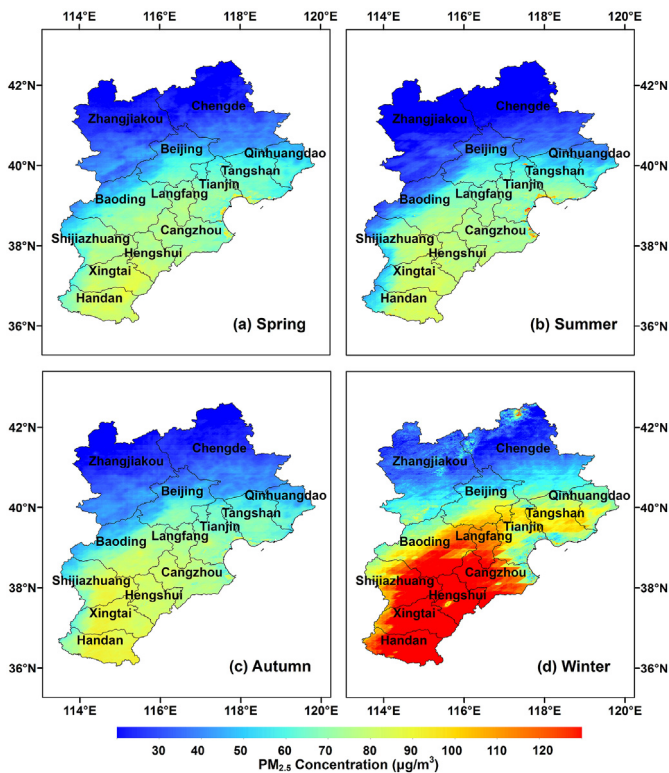
Fig. 3. Spatial distribution of the seasonal mean PM$_{2.5}$ concentrations from 2000 to 2018 in the BTH region.
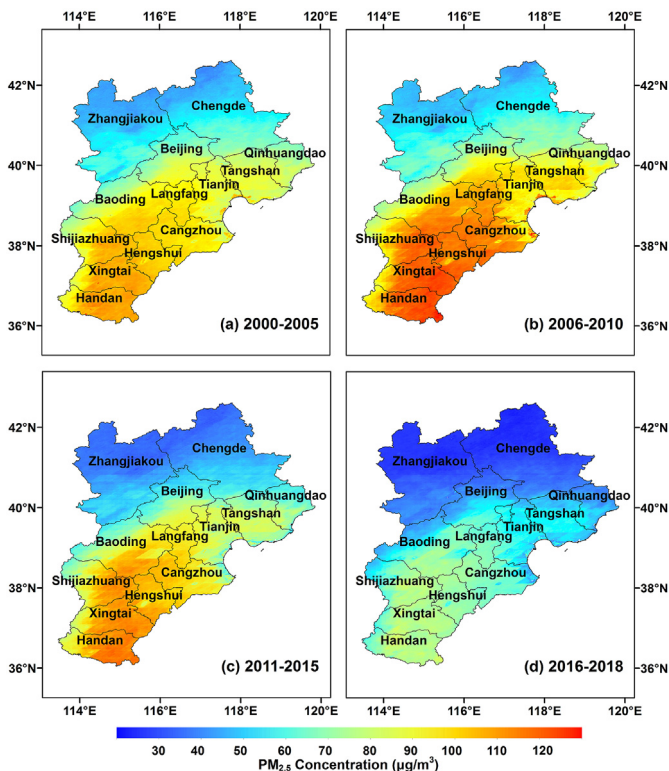

Fig. 4. Spatial distribution of the annual mean PM$_{2.5}$ concentration in the BTH region during the periods of (a) 2000–2005, (b) 2006–2010, (c) 2011–2015, and (d) 2016–2018.

35 μg/m^3, and the mean PM$_{2.5}$ concentration was 49.79 μg/m^3 in the BTH region. This phenomenon was mainly attributed to the rigorously implemented coordinated environmental development (Zhang et al., 2016). Moreover, the foundation for development was also built through environmental constraints in the 13th FYP. The mean PM$_{2.5}$ concentration was 71.90 μg/m^3 in the 12th FYP, which was much lower than that in the 11th FYP. Since 2011, the BTH region has been actively transforming its industrial structure and rigorously promoting the use of clean energy. Especially in September 2013, the action plan for the prevention and control of air pollution was launched and implemented by the China State Council. This has laid a solid foundation for air pollution control in the BTH region.

4.4. Long-term variations from 2000 to 2018

Fig. 5 shows the deseasonalized monthly anomaly trends of the PM$_{2.5}$ concentration from 2000 to 2018 in BTH and its main districts. There was a significant downward trend during this period, with the area of decrease (trend < 0; $p < 0.05$) accounting for 99.9% of the entire BTH region (Fig. 5e). The most substantial declines occurred in the eastern and southern areas, including Qinhuangdao, Tangshan, Tianjin, Cangzhou and Handan. In addition, the decreasing trends from 2000 to 2018 were calculated for the whole BTH region (−1.53 μg/m^3/year), Beijing (−1.58 μg/m^3/year), Tianjin (−1.85 μg/m^3/year) and Hebei province (−1.50 μg/m^3/year). The decreasing trends were all significant ($p < 0.05$). The temporal variation in PM$_{2.5}$ across the BTH region can be divided into three-time intervals, i.e., increasing (2000−2007), stable (2008−2012) and decreasing (2013−2018) phases. In the first phase, with the successful bid of the 28th Olympic Games, substantial economic production activities were carried out across the whole BTH region. Especially in Tianjin, the increasing PM$_{2.5}$ trend was 2.84 μg/m^3/year, which was 1.97 and 1.71 times as much as those in Beijing and Hebei province. The increasing trends were all significant at the 99% ($p < 0.01$) confidence level.

In the second phase, although the PM$_{2.5}$ concentration showed a decreasing trend (−1.60 μg/m^3/year) across the BTH region, statistical significance was not achieved ($p > 0.1$). Among the main districts, the trends of Beijing and Tianjin were significant, with downward trends of −3.02 μg/m^3/year ($p < 0.05$) and −3.47 μg/m^3/year ($p < 0.05$), respectively. However, the downward trend was not significant in Hebei province at the 90% ($p > 0.1$) confidence level. The main reason is that the secondary industry accounts for a high proportion of production in Hebei province, and a large number of industrial parks have been established (Li et al., 2018). Although the local government has implemented air pollution control measures, the downward trend is not significant. In the third phase, due to the implementation of environmental control policies and the enhancement of collaborative governance, the PM$_{2.5}$ concentration decreased rapidly. The trend in Hebei province decreased most notably, at −7.02 μg/m^3 per year ($p < 0.01$). In addition, the downtrends were −5.33 ($p < 0.01$), −6.31 ($p < 0.01$) and −6.83 μg/m^3/year ($p < 0.01$) in Beijing, Tianjin and the whole BTH region, respectively. The temporal variations in PM$_{2.5}$ indicated that the air quality in BTH has improved dramatically over the years.

5. Response of PM$_{2.5}$ to the industrial structure

5.1. Industrial emissions intensity

The industrial emissions intensity, i.e., the ratio of the industrial emissions to the GDP, can indicate the industrial technology level.
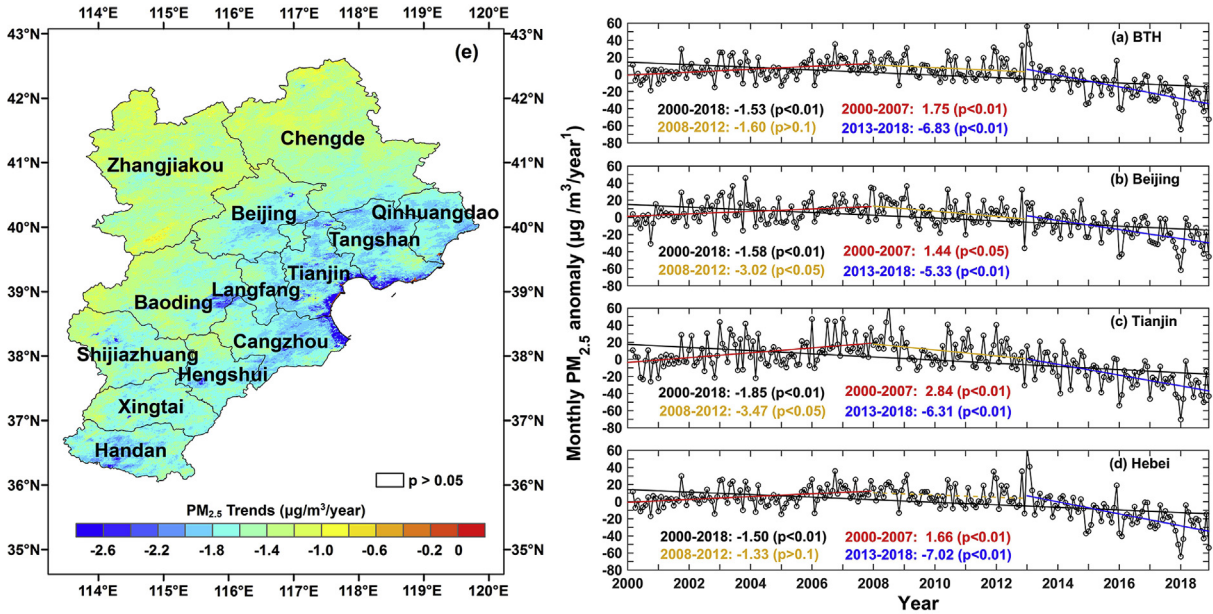
Fig. 5. Spatial distribution (e) of the PM$_{2.5}$ trend and time series of the monthly PM$_{2.5}$ anomalies in the (a) BTH region, (b) Beijing, (c) Tianjin, and (d) Hebei province.
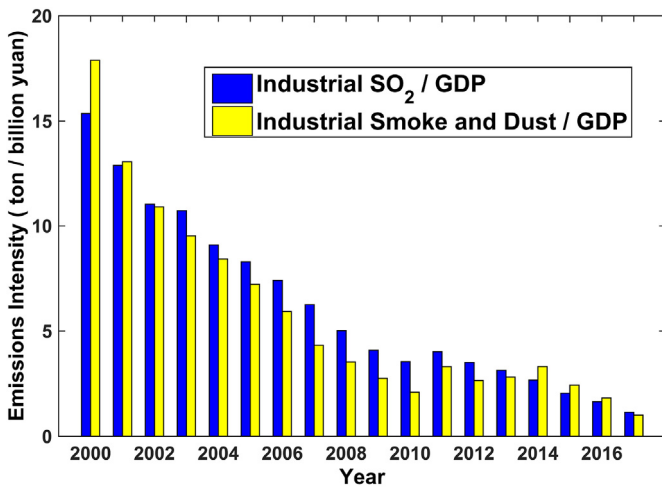

Fig. 6. The industrial emissions intensities in the BTH region from 2000 to 2017.

Fig. 6 shows the industrial emissions intensity in the BTH region from 2000 to 2017. An accelerated downward trend is observed in the BTH region. The wide use of desulfurization equipment and the effective management of smoke plumes in factories in those years are the reasons for the decline in the emissions intensity (Shi et al., 2017). In general, the decreasing trends of the SO$_2$ and smoke-dust emissions intensities are synchronous, and the changes in the smoke-dust emissions intensity were slightly more significant than those in the SO$_2$ emissions intensity, with an annual average change ratio of 16.44% (the ratio was 14.97% for the SO$_2$ emissions intensity). Notably, the fluctuation was captured from 2011 to 2014. The main cause of this phenomenon was the intensive economic development during this period in BTH. Due to the rapidly increasing technological innovations in BTH, the oscillation was slight. Although the industrial exhaust emission intensity has progressively declined, the changes in PM$_{2.5}$ fluctuated in BTH, especially from 2000 to 2013. Therefore, the industrial structure changes also need to be considered.

5.2. Industrial structure in the GDP and ADF tests

Fig. 7 shows the SI and TI proportions in the GDP of the BTH region from 2000 to 2017. Among all BTH regions, Beijing had the largest TI proportion and smallest SI proportion in the GDP, with mean values of 71.47% and 25.22%, respectively, from 2000 to 2017. The TI ratios in the GDP have always been higher than the SI ratios. The opposite situation was observed in Hebei province—the TI proportion was smaller than the SI proportion in the GDP. The mean TI and SI proportions were 35.56% and 51.28%, respectively. For Tianjin, the SI and TI proportions in the GDP were similar in most years. From 2000 to 2014, the SI ratio was higher than the TI ratio in the GDP. Then, with the development of science and technology in
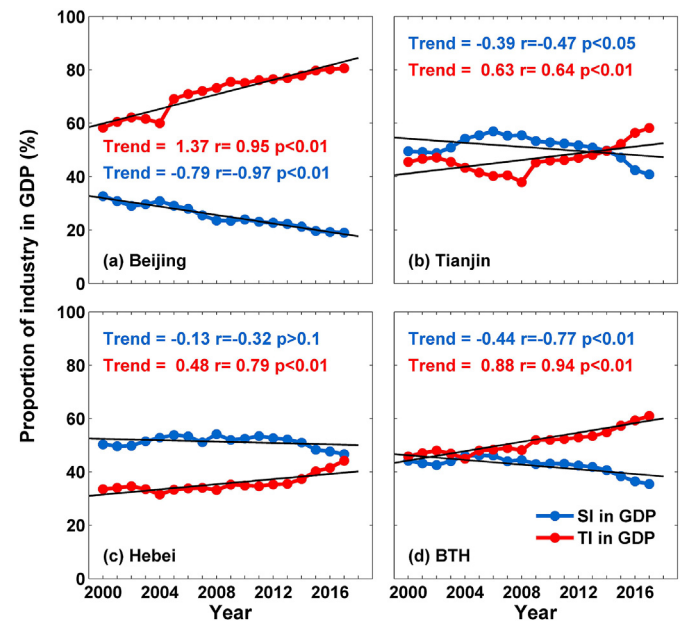

Fig. 7. The proportions of the secondary and tertiary industries in GDP in (a) Beijing, (b) Tianjin, (c) Hebei and (d) the BTH region from 2000 to 2017.

this area, the TI proportion exceeded the SI proportion in the GDP, reaching 58.2% in 2017. A striking dividing point was observed in the BTH region in 2008. After 2008, the TI proportion was significantly larger than the SI proportion in the GDP. This was most likely due to the Beijing 2008 Olympic Games, transforming the industrial structure. Although the SI and TI proportions in the GDP were different across the BTH region, the trends of those proportions remained consistent in the different areas. An upward trend was observed for the TI proportion in GDP, with trends of 1.34%, 0.63%, 0.48% and 0.88% for Beijing, Tianjin, Hebei and the whole BTH region, respectively. The confidence coefficient p values were all less than 0.01. For the SI ratio in the GDP, a significant downward trend existed in BTH, with a trend of -0.77% ($p < 0.01$).

In addition, the relationships between the $PM_{2.5}$ concentrations and the SI and TI proportions in GDP were calculated (Table S4). The results show that the relationships between the $PM_{2.5}$ concentration and industrial structure ratio are overall inconsistent in the BTH region. Tianjin showed the closest relationship, with correlation coefficients R of 0.92 ($p < 0.01$) and -0.93 ($p < 0.01$) for SI and TI, respectively. In addition, significant positive and negative effects on the $PM_{2.5}$ concentration ($p < 0.01$) caused by SI and TI were observed in Hebei. However, the relationships were not significant in Beijing ($p > 0.05$), suggesting the influence of other factors. Nevertheless, the industrial structure ratio plays an important role in the $PM_{2.5}$ concentration across the BTH region, with $R_{SI} = 0.84$ ($p < 0.01$) and $R_{TI} = -0.72$ ($p < 0.01$). Therefore, the VAR model was used in this study to analyze the dynamic response of $PM_{2.5}$ to the industrial structure in BTH. Initially, the ADF test was used in this paper to avoid spurious regression (Table S5). The significance levels were 90%, 99% and 99% for SI, TI and $GPM_{2.5}$, respectively. This indicates that the quarterly SI, TI and $GPM_{2.5}$ were all stationary, and those three variables can be used to build the VAR model.

5.3. Results of the VAR model

5.3.1. Model stability

Table 1 lists the results of the five criteria, and the suitable lag order for each criterion is marked in this table. Four of the five criteria, LR, FPEM AIC and HQIC, indicated that a lag order of 4 was optimal for this VAR model. In contrast, only SC indicated that a lag order of 2 was optimal. In addition, this also indicated that the time series of the variables met the requirements of establishing the VAR model. Therefore, the VAR (4) model was constructed in this work. In addition, a robustness test was also performed on this model, and its results are shown in Fig. S3. The reciprocals of all characteristic roots for the VAR model appeared within the unit circle, which indicates that this model is stable. The model could be used to perform the Granger causality test and impulse response analysis.

5.3.2. Granger causality test

The Granger causality test among $GPM_{2.5}$, SI and TI was used in this paper to understand the potential causal relationships between these three variables. Table 2 shows the results of the Granger causality test. It can be seen that SI ($p = 0.07$) and TI ($p = 0.005$) are both Granger causes for $GPM_{2.5}$. This indicates that changes in the industrial structure in terms of the SI and TI will affect the air quality. The reason for this is that changes in the industrial added value influence the total demand for fossil fuel use, e.g., the reduced use of coal in power plants and the heat production industry. In addition, the widespread use of clean energy could also reduce air pollution, i.e., natural gas and wind energy. Moreover, changes in the $GPM_{2.5}$ ($p = 0.005$) and TI ($p < 0.001$) will also cause structural SI changes. This indicates that the changes in the $PM_{2.5}$ concentration counteracted government environmental regulations and promoted the reform of industrial enterprises and, ultimately, structural SI changes in the long term.

5.3.3. Impulse response function

In the VAR model, the dynamic effects among $GPM_{2.5}$, SI and TI could be better interpreted according to the impulse response function. Fig. 8 shows the mutual responses or interactions among these three variables. The horizontal ordinate represents the number of lag periods of the response, and the vertical axis indicates the impulse responses of the dependent variables caused by the independent variables. The blue lines represent the impulse response function, and the shaded areas indicate two standard deviations. According to the Granger causality test results, four responses were selected for analysis in this study, i.e., $GPM_{2.5}$ to SI, $GPM_{2.5}$ to TI, SI to $GPM_{2.5}$ and SI to TI. In addition, 1- to 10-lag periods were used to reflect the impulse responses.

For the dynamic relationship between $GPM_{2.5}$ and SI (Fig. 8a), an increasing negative response occurred in the 1- to 4-lag periods, with the responses ranging from 0 to -0.0003. Although a positive response occurred in the fifth lag period, it quickly became negative, which lasted and remained steady for 5 lag periods. This indicates that industrialization has a positive impact on air pollution control in both the short and long terms. The reason for this effect might be that the development of industrialization has promoted an increase in the GDP. In addition, changes in the energy structure were also accompanied by an increase in SI, which promoted declines in the $PM_{2.5}$ concentration and $GPM_{2.5}$. However, this process is convoluted, and it cannot be achieved overnight.

Similar to the case for SI, a significantly negative response of $GPM_{2.5}$ to TI (Fig. 8b) occurred in the 1- to 3-lag periods (0 to -0.0004). Then, in the fourth lag period, a positive response (0.0003) appeared. However, the response of $GPM_{2.5}$ to TI decreased rapidly in the next lag (-0.0005), and it remained negative in the next 5- to 10-lag periods. On the one hand, a crowding effect on industrialization appeared to accompany the increase in TI. This phenomenon could promote the transfer of labor and capital from SI to TI. This will reduce the pollutant emissions and improve the environment. On the other hand, the increase in TI will also drive a rise in the GDP. This could result in a long-term and stable negative response of $GPM_{2.5}$ to TI.

The responses of SI to $GPM_{2.5}$ and TI were also calculated in this

Table 1
The selection results of the lag order in the VAR model, where * indicates the lag order according to the criterion.

Lag	LogL	LR	FPE (10^{-12})	AIC	SC	HQIC
0	531.495	NA	35.600	-15.544	-15.446	-15.505
1	659.328	240.625	1.080	-19.039	-18.647	-18.883
2	683.078	42.610	0.702	-19.473	$-18.787*$	-19.201
3	687.454	7.465	0.808	-19.337	-18.358	-18.949
4	718.527	50.266*	0.426*	$-19.986*$	-18.713	$-19.482*$

Table 2
Granger causality test results for $GPM_{2.5}$, SI and TI.

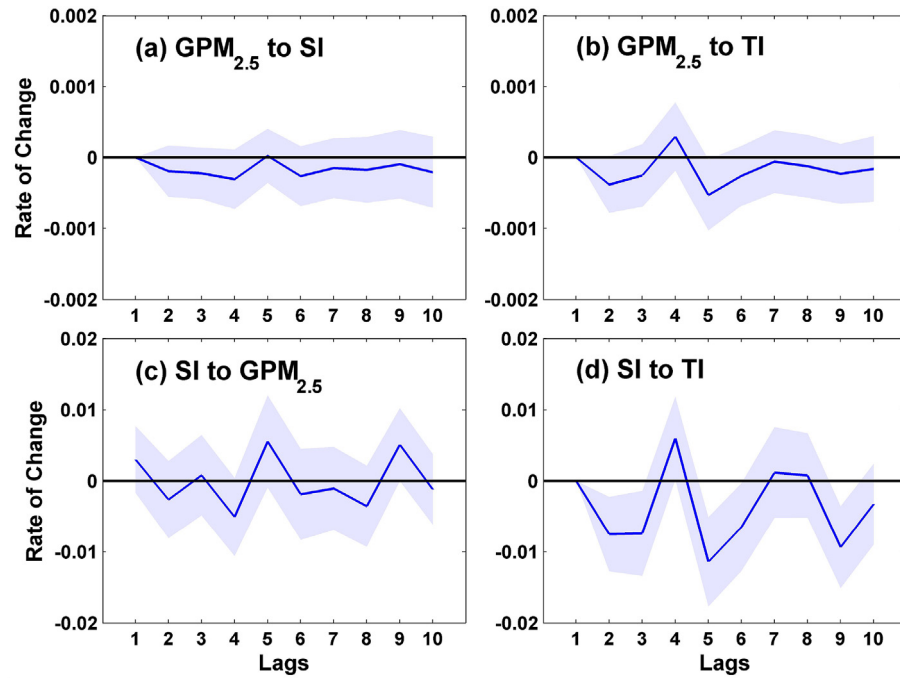| Equation	Excluded	Chi-squared	Degrees of freedom (df)	Probability
$GPM_{2.5}$	SI	8.665	4	0.070
$GPM_{2.5}$	TI	15.022	4	0.005
SI	$GPM_{2.5}$	14.936	4	0.005
SI	TI	37.116	4	< 0.001
TI	$GPM_{2.5}$	7.730	4	0.102
TI	SI	5.318	4	0.256
	All	21.314	8	0.006

Fig. 8. The responses of GPM$_{2.5}$ to SI (a), GPM$_{2.5}$ to TI (b), SI to GPM$_{2.5}$ (c) and SI to TI (d).

study. A fluctuating trend was observed in the response of SI to GPM$_{2.5}$ (Fig. 8c), and it exhibited alternating positive and negative changes in general. The minimum and maximum responses occurred in the 4-lag (-0.0051) and 5-lag (0.0055) periods, respectively. Since the planning of the secondary industry in the BTH area is often subject to compulsory government intervention, the impact mechanism of GPM$_{2.5}$ on SI is complex. This would also cause uncertainties in the response of SI to GPM$_{2.5}$.

Fig. 8d shows the impulse response spectrum between SI and TI. Positive responses were found in the 4-, 7- and 8-lag periods, and the other lag periods exhibited negative responses. The response trend suggests that increasing TI would reduce SI in the short term, and this might be consistent with the expectations of the Chinese government. In contrast, increasing TI could also promote SI in the medium term, especially in the 4-lag period ($\sim$0.0065). However, this promotion ability is limited, and the response became negative again in the 5-lag period and reached a steady state in the 9- and 10-lag periods ($\sim$$-$0.0028). This is consistent with the current policy of integrating the development of primary, secondary and tertiary industries.

5.3.4. Variance decomposition

Variance decomposition is an important part of the VAR model and is mainly used to determine the contributions of structural impacts on the changes of endogenous variables (Campbell and Ammer, 1993). Therefore, it is selected to reveal the dynamic characteristics between GPM$_{2.5}$ and the industrial structure and to analyze the contributions of structural shocks of SI and TI to GPM$_{2.5}$. Table 3 summarizes the variance decomposition results for GPM$_{2.5}$, SI and TI. These results indicated that the fluctuation in GPM$_{2.5}$ was significantly influenced by the added values of SI and TI. In the 1-lag period, the impact of SI and TI on GPM$_{2.5}$ was little. However, the influences of SI and TI diverged with increasing lag periods. The contribution rate of SI increased rapidly from the 1- to 3-lag periods and stabilized from the fourth lag period, at approximately 3.80%. The contribution rate of TI first increased and then decreased, reaching a peak of approximately 9.75% in the 5-lag period. Despite

Table 3
Variance decomposition results for the different variables.

Lags	Standard error	GPM$_{2.5}$ (%)	SI (%)	TI (%)
1	0.0015	100	0	0
2	0.0017	93.571	1.315	5.114
3	0.0020	92.664	2.155	5.181
4	0.0022	89.804	3.884	6.312
5	0.0024	87.144	3.703	9.753
6	0.0026	86.923	3.689	9.388
7	0.0027	87.613	3.699	8.688
8	0.0028	87.850	3.840	8.310
9	0.0030	88.298	3.578	8.124
10	0.0031	88.242	3.836	7.921

this phenomenon, the impacts of both SI and TI on GPM$_{2.5}$ gradually increased over time, which is in line with expectations. Compared with SI, TI has a greater impact on GPM$_{2.5}$, and the effect is gradually enhanced with increasing lag periods. This occurs because the main energy-consuming industries of SI are concentrated in the mining and manufacturing sectors, which are closely related to life in China, and the associated potential for controlling air pollution is limited. In addition, the contribution of the supply-side reform of TI to air pollution reduction is also very prominent.

6. Policy implications

At present, the core objective in the BTH region is to maintain the balance between economic development and air pollution reduction; thus, we put forward several policy suggestions. First, traditional industries have experienced extensive growth modes with low energy utilization and high consumption, leading to severe air pollution in the BTH region. On the one hand, we should use technological innovation and scientific management to actively adjust the industrial structure and guide the development of new clean industries. Clean industries, including new energy vehicles, industrial energy conservation and emissions reduction, circular economy, and resource recovery strategies, will have broad

development prospects. On the other hand, in terms of resource complementarity, the unreasonable industrial structure can be eliminated by building a regional cooperation system. Meanwhile, we should adjust the economic and energy structures, effectively control pollutant emissions, and promote the coordinated development of energy and the environment.

Second, we should establish an interest balance and compensation mechanism in the BTH region. Industrial upgrading and transformation require cooperation between governments, wherein the key is to coordinate interests, especially in the game relationship between local governments and enterprises. For example, most pillar industries in Hebei province are heavy industries with high pollution and emissions. The profit tendency of enterprises makes it difficult to close factories or change the existing industrial structure. Therefore, it is difficult to win the cooperation of enterprises if the emissions reduction policy on air pollution cannot establish a compensation mechanism for interests. Moreover, to promote the application of clean energy to enterprises, the government should increase the support policies, such as by increasing the subsidies and reducing the costs of using clean energy.

Last, the synergy between low carbon promotion and pollution control should be strengthened. Low-carbon technology refers to new technologies that can effectively control greenhouse gas emissions, including energy conservation and clean and renewable energy. The government should make a long-term development plan and give priority to the development of new clean and low-carbon technologies. Enterprises should be encouraged to invest in the development of clean and low-carbon technologies and the production of low-carbon energy. Then a complete clean economic development system for low-carbon agriculture, industry, and service industry can be gradually formed. In addition, we should strengthen international cooperation and the exchange of low-carbon and clean technologies, actively participate in low-carbon development around the world, and try to explore cleaner development methods.

7. Conclusions

Recently, the Beijing-Tianjin-Hebei (BTH) region in China has experienced severe air pollution episodes over the past years, and an increasing number of studies have focused on exploring the potential impact and response mechanism of $PM_{2.5}$ in different fields. However, the current satellite-derived $PM_{2.5}$ data sets have coarse spatial resolutions (3−50 km) and poor quality, as limited by the widely used aerosol optical depth (AOD) products. Aimed at these problems and based on the new high-resolution and high-quality Multiangle Implementation of Atmospheric Correction AOD products, a historical $PM_{2.5}$ data set at a higher 1 km resolution from 2000 to 2018 was first reconstructed using the linear mixed effect model in the BTH region. The spatiotemporal variations in $PM_{2.5}$ pollution and its response to the industrial structure during the last two decades were fully investigated.

Our results indicated that the model performs well in daily $PM_{2.5}$ estimates, with a high CV-R^2 of 0.85 and a small RMSE of 21.49 $\mu g/m^3$, and can well capture the historical $PM_{2.5}$ variations (e.g., monthly $R^2 = 0.72$) in the BTH region. High $PM_{2.5}$ concentrations are mainly observed in the southeast urban areas, where human activities are concentrated, while low values are found in the northwest vegetated areas. In general, $PM_{2.5}$ pollution has shown a significant decreasing trend by 1.53 $\mu g/m^3$/year (p < 0.01) from 2000 to 2018 in the BTH region, especially since 2013 (i.e., trend = −6.83 $\mu g/m^3$/year, p < 0.01). In addition, both secondary industry (SI) and tertiary industry (TI) showed significantly negative effects on $GPM_{2.5}$ from a long-term perspective, and

approximately 9.8% and 3.8% of the $GPM_{2.5}$ changes can be explained by the TI and SI, respectively. Therefore, the reform of the tertiary industry may be more effective for the prevention and control of air pollution in the future.

Although the $PM_{2.5}$ dataset produced in this paper shows high overall accuracy, because it is limited by the statistical regression model, the estimation and prediction ability of the model still has some deviation, which may lead to certain differences in historical $PM_{2.5}$ concentrations between satellite observations and the real situation. In addition, only the influence of the industrial structure in various economic factors on $PM_{2.5}$ pollution is considered in the current study. Therefore, in our future research, we will comprehensively consider the impacts of different factors on $PM_{2.5}$ pollution. Moreover, we will try to develop more accurate $PM_{2.5}$ remote-sensing estimation methods and expand the research scale to the national level to generate long-term series of high-resolution and high-quality $PM_{2.5}$ data set in China. This will be of great importance for future economic and health research on $PM_{2.5}$ pollution.

Credit author statement

Wenhao Xue: Writing - original draft, carried out the research and wrote the initial draft. All authors contributed to the interpretation of the results. **Jing Zhang:** designed the research. All authors contributed to the interpretation of the results. **Chao Zhong:** Data curation, Formal analysis, helped collect data and make the analysis. All authors contributed to the interpretation of the results. **Xinyao Li:** Data curation, Formal analysis, helped collect data and make the analysis. All authors contributed to the interpretation of the results. **Jing Wei:** designed the research. All authors contributed to the interpretation of the results.

Declaration of competing interest

The authors declare that they have no known competing financial interests or personal relationships that could have appeared to influence the work reported in this paper.

Acknowledgments

Appendix A. Supplementary data

Supplementary data to this article can be found online at https://doi.org/10.1016/j.jclepro.2020.123742.

References

Bei, N., Wu, J., Elser, M., Feng, T., Cao, J., Elhaddad, I., et al., 2017. Impacts of meteorological uncertainties on the haze formation in Beijing-Tianjin-Hebei (BTH) during wintertime: a case study. Atmos. Chem. Phys. 17 (23), 14579−14591.

Campbell, J.Y., Ammer, J., 1993. What moves the stock and bond markets? A variance decomposition for long-term asset returns. J. Finance 48 (1), 3−37.

Cavaliere, G., Xu, F., 2014. Testing for unit roots in bounded time series. J. Econom. 178, 259−272.

Chen, J., Yuan, H., Tian, X., Zhang, Y., Shi, F., 2019. What determines the diversity of CO_2 emission patterns in the Beijing-Tianjin-Hebei region of China? An analysis focusing on industrial structure change. J. Clean. Prod. 228, 1088−1098.

Dee, D.P., Uppala, S.M., Simmons, A.J., Berrisford, P., Poli, P., Kobayashi, S., Vitart, F., 2011. The ERA-interim reanalysis: configuration and performance of the data assimilation system. Q. J. R. Meteorol. Soc. 137 (656), 553−597.

Ding, Y., Zhang, M., Chen, S., Wang, W., Nie, R., 2019. The environmental Kuznets curve for PM2.5 pollution in Beijing-Tianjin-Hebei region of China: a spatial panel data approach. J. Clean. Prod. 220, 984–994.

Gao, J., Wang, K., Wang, Y., Liu, S., Zhu, C., Hao, J., et al., 2018. Temporal-spatial characteristics and source apportionment of PM2.5 as well as its associated chemical species in the Beijing-Tianjin-Hebei region of China. Environ. Pollut. 233, 714–724.

Granger, C.W.J., 1969. Investigating causal relations by econometric models and cross-spectral methods. Econometrica 37 (37), 424–438.

Granger, C.W.J., Newbold, P., 1974. Spurious regressions in econometrics. J. Econom. 2 (2), 111–120.

Gupta, J., Vegelin, C., 2016. Sustainable development goals and inclusive development. Int. Environ. Agreements Polit. Law Econ. 16, 433–448.

He, Q., Huang, B., 2018. Satellite-based mapping of daily high-resolution ground PM2.5 in China via space-time regression modeling. Rem. Sens. Environ. 206, 72–83.

Hurvich, C.M., Tsai, C.L., 1993. A corrected Akaike information criterion for vector autoregressive model selection. J. Time Anal. 14 (3), 271–279.

Kohavi, R., 1995. A study of cross-validation and bootstrap for accuracy estimation and model selection. In: Ijcai. Canada, Montreal, pp. 1137–1145.

Lee, H.J., Liu, Y., Coull, B.A., Schwartz, J., Koutrakis, P., 2011. A novel calibration approach of MODIS AOD data to predict PM2.5 concentrations. Atmos. Chem. Phys. Discuss. 11 (3).

Li, T., Shen, H., Yuan, Q., Zhang, X., Zhang, L., 2017. Estimating ground-level PM2.5 by fusing satellite and station observations: a geo-intelligent deep learning approach. Geophys. Res. Lett. 44 (23), 11–985.

Li, W., An, C., Lu, C., 2018. The assessment framework of provincial carbon emission driving factors: an empirical analysis of Hebei Province. Sci. Total Environ. 637, 91–103.

Li, X., Zhang, Q., Zhang, Y., Zheng, B., Wang, K., Chen, Y., et al., 2015. Source contributions of urban PM2.5 in the Beijing–Tianjin–Hebei region: changes between 2006 and 2013 and relative impacts of emissions and meteorology. Atmos. Environ. 123, 229–239.

Luo, K., Li, G., Fang, C., Sun, S., 2018. PM2.5 mitigation in China: socioeconomic determinants of concentrations and differential control policies. J. Environ. Manag. 213, 47–55.

Lyapustin, A., Wang, Y., Korkin, S., Huang, D., 2018. MODIS Collection 6 MAIAC algorithm. Atmos. Meas. Tech. 11 (10).

Lütkepohl, H., 1985. Comparison of criteria for estimating the order of a vector autoregressive process. J. Time Anal. 6 (1), 35–52.

Ma, Z., Hu, X., Sayer, A., Levy, R., Zhang, Q., Liu, Y., 2016. Satellite-based spatiotemporal trends in PM2.5 concentrations: China, 2004–2013. Environ. Health Perspect. 124 (2), 184–192.

Ma, Z., Hu, X., Sayer, A.M., Levy, R., Zhang, Q., Xue, Y., Tong, S., Bi, J., Huang, L., Liu, Y., 2015. Satellite-based spatiotemporal trends in PM2.5 concentrations: China, 2004–2013. Environ. Health Perspect. 124, 184–192.

Neter, J., Kutner, M.H., Nachtsheim, C.J., Wasserman, W., 1996. Applied Linear Statistical Models. Irwin Chicago.

Rohde, R.A., Muller, R.A., 2015. Air pollution in China: mapping of concentrations and sources. PLoS One 10, e0135749.

Shi, W., Lin, C., Chen, W., Hong, J., Chang, J., Dong, Y., et al., 2017. Environmental effect of current desulfurization technology on fly dust emission in China. Renew. Sustain. Energy Rev. 72, 1–9.

Sims, C.A., 1972. Money, income, and causality. Am. Econ. Rev. 62 (62), 540–552.

Song, W., Jia, H., Huang, J., Zhang, Y., 2014. A satellite-based geographically weighted regression model for regional PM2.5 estimation over the Pearl River Delta region in China. Rem. Sens. Environ. 154, 1–7.

Song, Y., Huang, B., He, Q., Chen, B., Wei, J., Mahmood, R., 2019. Dynamic assessment of PM2.5 exposure and health risk using remote sensing and geo-spatial big data. Environ. Pollut. 253, 288–296.

Tian, Y., Jiang, Y., Liu, Q., et al., 2019. Temporal and spatial trends in air quality in Beijing. Landsc. Urban Plann. 185, 35–43.

Wang, X., Dickinson, R.E., Su, L., Zhou, C., Wang, K., 2018. PM2.5 pollution in China and how it has been exacerbated by terrain and meteorological conditions. Bull. Am. Meteorol. Soc. 99 (1), 105–119.

Wei, J., Huang, W., Li, Z., Xue, W., Peng, Y., Sun, L., Cribb, M., 2019a. Estimating 1-km-resolution PM2.5 concentrations across China using the space-time random forest approach. Rem. Sens. Environ. 231, 111221.

Wei, J., Li, Z., Cribb, M., Huang, W., Xue, W., Sun, L., Guo, J., Peng, Y., Li, J., Lyapustin, A., Liu, L., Wu, H., Song, Y., 2020. Improved 1 km resolution PM2.5 estimates across China using enhanced space-time extremely randomized trees. Atmos. Chem. Phys. 20 (6), 3273–3289.

Wei, J., Li, Z., Guo, J., Sun, L., Huang, W., Xue, W., Fan, T., Cribb, M., 2019b. Satellite-derived 1-km-resolution PM1 concentrations from 2014 to 2018 across China. Environ. Sci. Technol. 53 (22), 13265–13274.

Wei, J., Li, Z., Peng, Y., Sun, L., 2019c. MODIS Collection 6.1 aerosol optical depth products over land and ocean: validation and comparison. Atmos. Environ. 201, 428–440.

Wei, J., Li, Z., Peng, Y., Sun, L., Yan, X., 2019d. A regionally robust high-spatial-resolution aerosol retrieval algorithm for MODIS images over Eastern China. IEEE Trans. Geosci. Rem. Sens. 57 (7), 4748–4757.

Wei, J., Peng, Y., Mahmood, R., Sun, L., Guo, J., 2019e. Intercomparison in spatial distributions and temporal trends derived from multi-source satellite aerosol products. Atmos. Chem. Phys. 19 (10), 7183–7207.

Wei, J., Sun, L., Huang, B., Bilal, M., Zhang, Z., Wang, L., 2018. Verification, improvement and application of aerosol optical depths in China. Part 1: intercomparison of NPP-VIIRS and Aqua-MODIS. Atmos. Environ. 175, 221–233.

Wei, J., Sun, L., Peng, Y., Wang, L., Zhang, Z., Bilal, M., Ma, Y., 2018. An improved high-spatial-resolution aerosol retrieval algorithm for MODIS images over land. J. Geophys. Res. Atmos. 123 (21), 12291–12307.

Wu, J., Zheng, H., Zhe, F., Xie, W., Song, J., 2018. Study on the relationship between urbanization and fine particulate matter (PM2.5) concentration and its implication in China. J. Clean. Prod. 182, 872–882.

Xin, J., Gong, C., Liu, Z., Cong, Z., Gao, W., Song, T., Pan, Y., Sun, Y., Ji, D., Wang, L., 2016. The observation-based relationships between PM2.5 and AOD over China. J. Geophys. Res. Atmos. 121, 10–701.

Xue, W., Zhang, J., Qiao, Y., Wei, J., Lu, T., Che, Y., Tian, L., 2020. Spatiotemporal variations and relationships of aerosol-radiation-ecosystem productivity over China during 2001-2014. Sci. Total Environ. 741, 140324.

Xue, W., Zhang, J., Zhong, C., Ji, D., Huang, W., 2020. Satellite-derived spatiotemporal PM2.5 concentrations and variations from 2006 to 2017 in China. Sci. Total Environ. 712, 134577.

Yang, D., Wang, X., Xu, J., Xu, C., Lu, D., Ye, C., et al., 2018. Quantifying the influence of natural and socioeconomic factors and their interactive impact on PM2.5 pollution in China. Environ. Pollut. 241, 475–483.

Yang, Q., Yuan, Q., Li, T., Shen, H., Zhang, L., 2017. The relationships between PM2.5 and meteorological factors in China: seasonal and regional variations. Int. J. Environ. Res. Publ. Health 14 (12), 1510.

Yao, F., Wu, J., Li, W., Peng, J., 2019. A spatially structured adaptive two-stage model for retrieving ground-level PM2.5 concentrations from VIIRS AOD in China. ISPRS J. Photogrammetry Remote Sens. 151, 263–276.

You, W., Zang, Z., Pan, X., Zhang, L., Chen, D., 2015. Estimating PM2.5 in Xi'an, China using aerosol optical depth: a comparison between the MODIS and MISR retrieval models. Sci. Total Environ. 505, 1156–1165.

Zang, L., Mao, F., Guo, J., Gong, W., Wang, W., Pan, Z., 2018. Estimating hourly PM1 concentrations from Himawari-8 aerosol optical depth in China. Environ. Pollut. 241, 654–663.

Zhang, H., Hu, J., Qi, Y., Li, C., Chen, J., Wang, X., et al., 2017. Emission characterization, environmental impact, and control measure of PM2.5 emitted from agricultural crop residue burning in China. J. Clean. Prod. 149, 629–635.

Zhang, H., Wang, S., Hao, J., Wang, X., Wang, S., Chai, F., Li, M., 2016. Air pollution and control action in Beijing. J. Clean. Prod. 112, 1519–1527.

Zhang, J., Jiang, H., Liu, G., Zeng, W., 2018a. A study on the contribution of industrial restructuring to reduction of carbon emissions in China during the five Five-Year Plan periods. J. Clean. Prod. 176, 629–635.

Zhang, Y., Li, Z., 2015. Remote sensing of atmospheric fine particulate matter (PM2.5) mass concentration near the ground from satellite observation. Rem. Sens. Environ. 160, 252–262.

Zhang, X., Zhang, W., Lu, X., Liu, X., Chen, D., Liu, L., Huang, X., 2018b. Long-term trends in NO2 columns related to economic developments and air quality policies from 1997 to 2016 in China. Sci. Total Environ. 639, 146–155.